Density Functional Based Parametrization of a Valence Bond Method and Its Applications in Quantum-Classical Molecular Dynamics Simulations of Enzymatic Reactions

P. GROCHOWSKI* AND B. LESYNG

Department of Biophysics, Warsaw University, Zwirki i Wigury 93, 02-089 Warsaw, Poland and Interdisciplinary Centre for Mathematical and Computational Modelling, Warsaw University, Banacha 2, 02-097 Warsaw, Poland; e-mail: pawelg@icm.edu.pl

P. BAŁA

Interdisciplinary Centre for Mathematical and Computational Modelling, Warsaw University, Banacha 2, 02-097 Warsaw, Poland and Institute of Physics, N. Copernicus University, Grudziądzka 5/7, 87-100 Toruń, Poland

J. A. McCAMMON

Department of Chemistry and Biochemistry, University of California at San Diego, La Jolla, California 92093-0365, USA

Received August 31, 1995; revised manuscript received November 13, 1995; November 14, 1995

ABSTRACT

An approximate valence bond (AVB) method was parametrized at a microscopic level for proton transfer and hydroxyanion nucleophilic reactions in enzyme catalytic processes. The method was applied to describe hydrolytic activity of phospholipase A_2. The AVB parametrization is based on density functional and conventional ab initio calculations calibrated with respect to experimental data in the gas phase. The method was used as a fast generator of the potential energy function in a quantum-classical molecular dynamics (QCMD) simulations describing atomic motions as well as propagation of the proton wave function in the enzyme active site. The protein environment surrounding the active site and solvent effects are included in the model via electrostatic interactions perturbing the original AVB Hamiltonian.

* To whom correspondence should be addressed.

International Journal of Quantum Chemistry, Vol. 60, 1143–1164 (1996)

CCC 0020-7608 / 96 / 061143-22

Introduction

The structure and dynamics of molecular and biomolecular systems like enzymes are often described using conventional molecular mechanics (MM) or molecular dynamics (MD) methods. In these models atoms are described as classical pointlike particles, moving on an effective Born–Oppenheimer potential surface. The potential energy surface is usually approximated as a sum of simple analytical functions, which depend on nuclear positions and are parametrized based on time-dependent, stationary quantum-mechanical calculations and/or experimental data. For review of the MM and MD methods as well as their applications see [1–3]. Conventional MM and MD methods usually assume fixed topological structures of molecules. A microscopic description of dissociation processes changing the topology of molecules is a challenging problem. Proton or electron transfer processes are even more complicated. The quantum-dynamical nature of these motions cannot be neglected. This, in particular, limits current studies of enzymatic reactions. A precise description of such processes requires application of the time-dependent Schrödinger equation.

Since enzymatic systems are usually large, they have to be divided into regions described at various approximation levels. The enzymatic structure forming the environment for the active site can be described using classical or implicitly quantum-mechanical theories (classical region). In most cases conventional potential energy function (PF) and MD models describe this region. The potential energy function for atoms in the active site, where the enzymatic reactions occur (quantum region), have to be numerically determined using quantum-mechanical methods or described using properly designed analytical potentials. Using the quantum-mechanical (QM) methods is more general. Taking this into account we selected a valence bond method as a fast generator of the potential energy surface. Assuming that the potential energy surface is known or can be generated, the motion of proton(s) or excess electron(s) in the enzyme active site is described in our model by the time-dependent Schrödinger equation (QD subsystem). The model is called quantum-classical molecular dynamics (QCMD); see [4–6] for details.

The valence bond (VB) method was first formulated by Heitler and London in 1927 for the H_2 molecule [7]. It was later developed by many quantum chemists, in particular by Pauling [8], Coulson and McWeeny, see e.g. [9], and Murell et al. [10]. During the past 15 years an empirical version of this method (EVB) has been developed and applied for chemical and biochemical reactions by Warshel and co-workers (see [11–18]), as well as by Robb and co-workers [19, 20]. Several other models which couple quantum and classical methods to generate effective potential energy functions for macromolecular studies were formulated, for example, by Karplus et al. [21] and Kollman et al. [22]. In turn quantum-dynamical models describing time-dependent proton and electron transfer processes in molecular and biomolecular systems were studied by Berendsen et al. [23], Alimi et al. [24], Hynes et al. [25, 26], Miller et al. [27, 28], Onuchic et al. [29], and Car and Parinello [30].

The purpose of this study is to formulate and parametrize an approximate valence bond (AVB) method that is consistent with the QCMD model [31]. We adopted the basic scheme of the EVB method of Warshel and co-workers [11, 12, 14] and developed it into a rigorously microscopic approach. The whole model used for quantum-classical molecular dynamics simulations is called QCMD/AVB. Its application to the quantum-dynamical proton transfer reaction and a nucleophilic attack process in an enzyme active site will be presented. There are two features which differ our model from the molecular dynamics models based on EVB. First, in our parametrization we do not use any macroscopic, thermodynamical parameters. The parametrization is based exclusively on microscopic quantum-mechanical, density functional, and conventional ab initio calculations and adjusted whenever possible to fit gas-phase experimental data. In the EVB method the influence of the environment is usually described based on thermodynamic quantities like the free energy of solvation. In a very limited way implementation of the EVB was also proposed for a model nucleophilic SN_2 reaction [15]. Until now no consistent and complete parametrization procedure was proposed based on ab initio or density functional theory (DFT) calculations.

Second, regarding the proton dynamics in the active site, we integrate explicitly the time-depen-

dent Schrödinger equation for the proton motion in parallel with the classical dynamics for other atoms. This accounts automatically for proton delocalization, its zero point energy, and tunneling effects. This model allows for simulations of the microscopic evolution in an enzyme active site over the time scale of 10^{-14}–10^{-9} s. Such treatment provides a direct insight into quantum-dynamical effects. One should note that in some studies, for example [16], quantum corrections for rate constants of diabatic and adiabatic reactions in solutions were introduced based on the classical dynamics governed by the EVB potential energy function.

The QCMD/AVB model is applied to phospholipase A_2. In the next section we describe the structure and function of this enzyme and define its classical and quantum regions. In the following sections we present the AVB method, its parametrization and implementation in the QCMD/AVB dynamics of the enzymatic reaction.

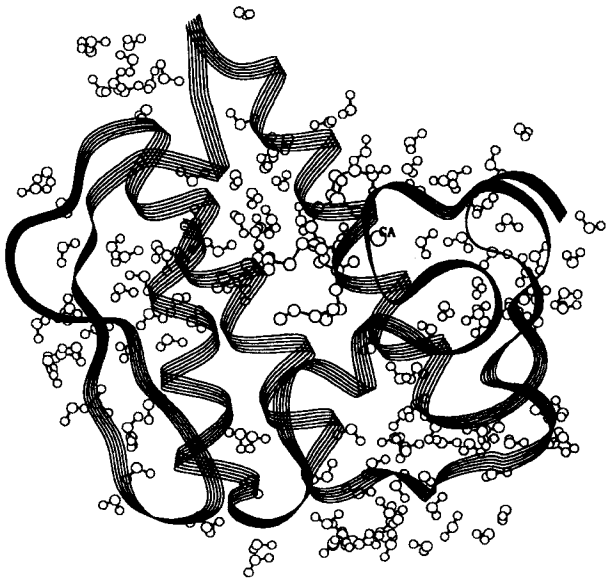

FIGURE 1. Crystallographic structure of PLA_2 [32]. The ribbon denotes the polypeptide chain. The inhibitor, water of hydration, and the calcium cation are shown using the ball-and-stick representation.

Phospholipase A_2, the Test Case for the QCMD/AVB Method

Phospholipase A_2 (PLA_2) is an enzyme which acts at a lipid-aqueous interface of biological membranes catalyzing the hydrolysis of phosphoglycerides. The enzyme is stereoselective and splits the ester bond at the 2-acyl group in L-1,2 diacylphosphatides. The crystal structures of the native and inhibited PLA_2 molecules from the Chinese cobra venom are available [32]. The enzymatic mechanism was also proposed [33].

The molecular system used in the simulation consists of the enzyme molecule with 118 residues, a substrate bonded in the enzyme active site, a calcium cation, and 147 water molecules of hydration (see Fig. 1). The total system contains about 1600 atoms (nonpolar hydrogens connected to carbons are not included, the *united atom* model is used). Figure 2 shows the chemical structure of the substrate and the phosphonate inhibitor used in the reported crystallographic data. The conformation of the inhibitor in the active site is similar to the tetrahedral intermediate state of the substrate molecule during the enzymatic reaction. In the native enzyme several water molecules are present in the active site. One of these molecules remains

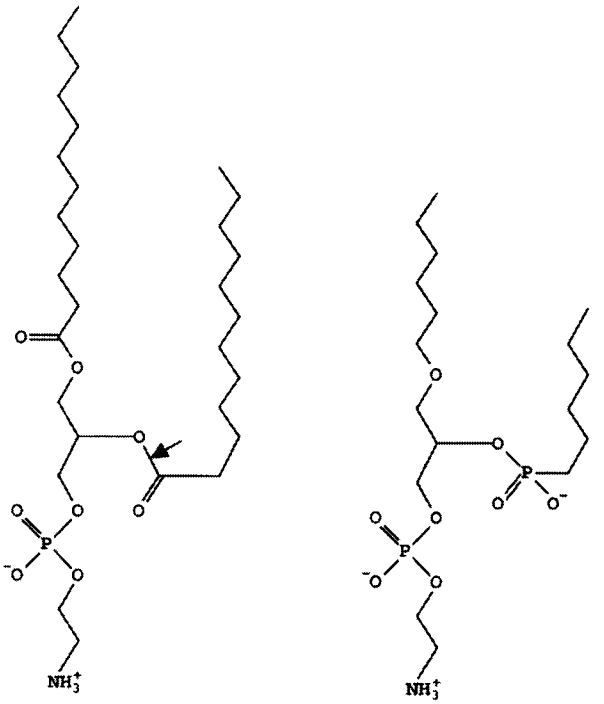

FIGURE 2. Chemical structures of the substrate and the inhibitor. The arrow points out the ester bond hydrolyzed by PLA_2. The inhibitor mimics the tetrahedral transition state during the enzymatic process.

in the site when the substrate is docked and is used in the hydrolysis process. This mechanism is presented in Figure 3. To build the model of the initial substrate–enzyme complex we replaced the PO_2^- group of the inhibitor by the CO group of the substrate and added one water molecule in a space between the substrate and the imidazole ring of His 48. The structure of the complex was first optimized by the energy minimization, then thermalized and equilibrated using a standard MD procedure (see [31]).

The quantum region described by the AVB method consists of the imidazole ring of His 48, the water molecule, and a fragment of the substrate containing the ester bond to be hydrolyzed. The remaining atoms of the substrate together with the whole protein environment belong to the classical region.

The AVB method was parametrized to describe the first two steps of the enzymatic reaction: the proton transfer between the water molecule and the imidazole ring and the nucleophilic attack of the resulting hydroxyanion on the substrate leading to an intermediate state with the tetragonal hybrydization of the carbonyl carbon [compare Fig. 3(b) and 3(c)]. In the reported QCMD/AVB simulations the proton in the water-imidazole hydrogen bond is described as the quantum-dynamical particle. The potential energy curve with respect to the proton transfer coordinate is bistable in the presence of the electrostatic field generated by the protein environment. This effect is illustrated in the following examples of the QCMD/AVB simulations.

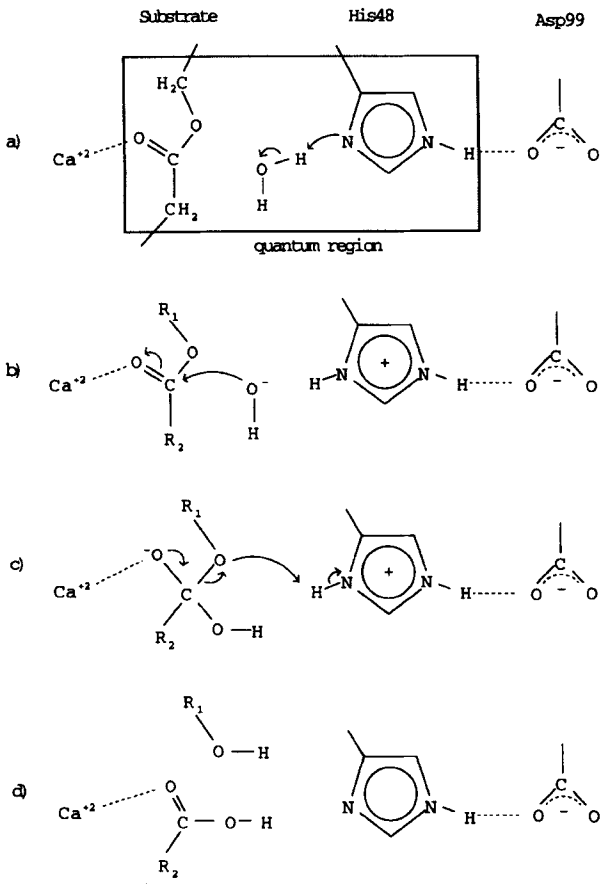

FIGURE 3. Enzymatic mechanism of the phosphoglyceride hydrolysis by PLA_2.

Principles of the AVB Method and Its Formulation for the Enzymatic Reaction

In the VB formalism the exact, many-electron wave function of a molecule is approximated as a mixture of wave functions representing canonical (valence bond) chemical structures. In turn, each structure is built up of localized orbitals. The orbitals can either be atomic orbitals (e.g., lone electron pairs) or superpositions of atomic orbitals from pairs of atoms. Those orbitals represent valence or ionic bonds. Assuming that we study the closed-shell systems all valence electrons are coupled into pairs and are assigned to these orbitals. For example, if a pair of electrons taken from two atoms is located exclusively on one of these atoms, we get two oppositely charged ions, which creates a ionic bond. Usually the occupation of atomic core orbitals is frozen, but the method can be extended to all electrons and atomic orbitals in the molecule. For review of the VB methods see e.g. [9, 10]. A single valence bond structure represents a limiting distribution of the electrons and corresponds to a particular electronic wave function ψ_i. The ground, many-electron state is approximated by a linear combination of these functions:

$$\Psi = \sum_i c_i \psi_i. \qquad (1)$$

Values of the c_i coefficients are determined by minimizing the total energy of the state Ψ,

$$E = \frac{\int \Psi^* \hat{H} \Psi \, d\tau}{\int \Psi^* \Psi \, d\tau}. \tag{2}$$

Application of the variational principle leads to a set of linear equations:

$$\sum_i (H_{ij} - ES_{ij})c_j = 0, \tag{3}$$

where H_{ij} and S_{ij} are the elements of the Hamiltonian and overlap matrices, respectively:

$$H_{ij} = \int \psi_i^* \hat{H} \psi_j \, d\tau, \tag{4}$$

$$S_{ij} = \int \psi_i^* \psi_j \, d\tau. \tag{5}$$

In general, the integrals can be evaluated with the aid of a mathematical representation of the atomic orbitals. In the case of approximate, empirical versions of the valence bond method one assumes validity of the explicit set of equations (3), but the valence structures $\{\psi_i\}$ do not need any mathematical representation. Following Warshel and coworkers we adopted a similar approach. The elements of the Hamiltonian as well as overlap matrix are calculated using empirical formulas and depend on relative positions of the atomic nuclei. The number of the VB structures used in the model is restricted by the computational costs and the knowledge of empirical parameters used in the parametrization of the Hamiltonian matrix. The potential energy surface of the molecular system is described by the lowest eigenvalue of the Hamiltonian matrix. Two examples of a two-state VB models are presented in Figures 4(a) and 4(b). The first figure shows a situation typical for description of dissociation process; the second one represents a simplified description of a proton transfer reaction in a bistable potential. Note that in the present study a more complicated model is used, and it will be shown that the bistable potential for the proton transfer appears in the presence of the electrostatic field generated by the protein environment.

In the current implementation of the VB method we assume orthogonality of the VB structures, $S_{ij} = \delta_{ij}$. The ground-state energy of the system is

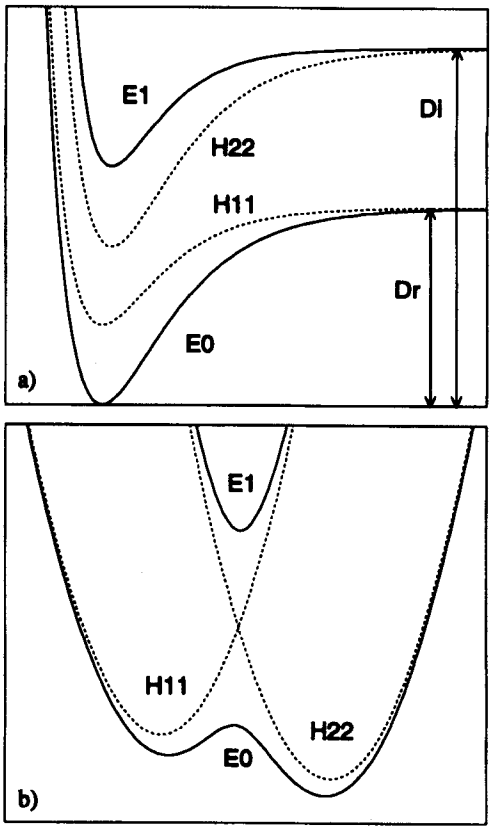

FIGURE 4. Schematic representation of a two-state AVB model. Both figures present the energy curves plotted with respect to a reaction coordinate. H_{11} and H_{22} are the diagonal elements of the Hamiltonian matrix. They represent energies of the system in the hypothetical states described by ψ_1 and ψ_2 electronic wave functions. E^0 and E^1 are the Born–Oppenheimer energy curves in the ground and first excited electronic state of the system. Figure (a) describes a typical situation for dissociation of chemical bonds. D_l and D_r are the energies for a ionic and a radical dissociation process, respectively. Figure (b) presents a reaction with a bistable potential of the ground electronic state.

the lowest eigenvalue of the Hamiltonian matrix:

$$\det(\mathbf{H} - \mathbf{I}E) = 0. \tag{6}$$

The expansion coefficients, c_i, are real numbers and can be calculated using the following system of equations:

$$\begin{cases} \Sigma_j (H_{ij} - \delta_{ij} E) c_j = 0 \\ \Sigma_j c_j^2 = 1 \end{cases}. \tag{7}$$

The quantum region of the PLA_2–substrate complex is described by the following VB structures:

1. $O = C\,HO - H\,Im$
2. $O = C\,HO^- H^+\,Im$
3. $O = C\,HO^-\,H - Im^+$
4. $^-O - C^+\,HO - H\,Im$
5. $^-O - C^+\,HO^- H^+\,Im$
6. $^-O - C^+\,HO^-\,H - Im^+$
7. $^-O - C - OH\,H^+\,Im$
8. $^-O - C - OH\,H - Im^+$

Im stands for the imidazole ring and O = C represents the following fragment of the substrate, $-CH_2 - CH_2 - CO - O - CH_2 -$. In the case of the native enzyme, without any substrate molecule, the above list is reduced to the first three structures. In the next section we will present analytical formulas used in the construction of the diagonal elements of the AVB Hamiltonian matrix for the quantum region extracted from the enzyme, in the vacuum state. This part of the parametrization procedure follows concepts of Warshel (see [14]). Next, we will describe a special case of a two-state AVB Hamiltonian for diatomic molecular fragments, perturbed by electrostatic interactions with the environment. This approach allows us to evaluate the nondiagonal Hamiltonian matrix elements and coupling terms describing interactions between the quantum and classical regions.

Analytical Representation of the Diagonal AVB Hamiltonian Matrix Elements

A diagonal element of the Hamiltonian matrix, H_{ii}, represents the total energy of a hypothetical electron distribution defined by its VB structure ψ_i at a given configuration of the atomic nuclei. This energy is approximated with an analytical PF in the form of a sum of elementary interaction potentials:

$$H_{ii} = V_i^0 + \sum V_i^{\text{bond}} + \sum V_i^{\text{ang}} + \sum V_i^{\text{tors}} + \sum V_i^{\text{impr}} + \sum V_i^{\text{es}} + \sum V_i^{\text{val}}. \quad (8)$$

V_i^0 are independent on the positions of the nuclei and describe the relative energies of the valence structures. They are usually calculated by considering the so-called asymptotic structures in which the molecular fragments are separated to infinity. The relative energies of the asymptotic structures can be determined by analyzing electron transfer between the separated molecules. Consider the proton dissociation from the water molecule. During the dissociation process the proton can either keep its electron or leave it at the OH group. This leads either to a biradical or an ionic asymptotic structure [compare Fig. 4(a)]. This means that the VB states ψ_1 and ψ_2, listed in the previous section, differ at long HO–H distance (and separation of other molecular fragments), being either in a biradical or a ionic form, respectively. Their energy difference is equal to the electron-transfer energy between OH^- and the proton. Using experimental data one can adjust the relative positions of asymptotic values of the diagonal matrix elements. This is a component of a more general adjustment procedure presented in the next section. The other terms in (8) have forms of approximate empirical potentials used in the PF approximation. These are, respectively, potentials of the bonds, bond angles, torsional angles, improper dihedral angles, as well as electrostatic and nonbonded valence interactions. The parameters used in these interaction potentials depend on the valence structures (for simplicity the indices which denote the VB structures have been omitted). The potential of a bond is described by a Morse function. Analytical forms of the interaction potentials are presented below (r, α, θ, and δ denote the bond length and the angles, respectively):

$$V^{\text{bond}}(r) = D_0[\exp a(r_0 - r) - 1]^2, \quad (9)$$

$$V^{\text{ang}}(\alpha, r) = A^{\text{ang}}(r)(\cos\alpha - \cos\alpha_0)^2, \quad (10)$$

$$V^{\text{tors}}(\theta, r) = A^{\text{tors}}(r)[1 - \cos n(\theta - \theta_0)], \quad (11)$$

$$V^{\text{impr}}(\delta, r) = A^{\text{impr}}(r)(\delta - \delta_0)^2. \quad (12)$$

Amplitudes $A(r)$ appearing in the angular potentials can be, in general, functions of the bond lengths adjacent to the angle. In the actual parametrization they are constants or depend exclusively on the "dissociable" bond:

$$A(r) = \begin{cases} A_0 \\ A_0 r \exp(-ar) \end{cases}. \quad (13)$$

The electrostatic and nonbonded valence interactions are calculated for all pairs of atoms in the structure which belong to separate molecules or are connected by three or more bonds (q_a and q_b denote effective atomic point charges placed on the nuclei of the atoms a and b, respectively, k is the Coulomb constant):

$$V^{es}(r) = k\frac{q_a q_b}{r}, \tag{14}$$

$$V^{val}(r) = \frac{B\exp(-br) - C}{r^6}. \tag{15}$$

In the case of interactions between the bare proton (H^+ in the schemes) and other atoms the nonbonded valence potential has a more specific form:

$$V^{val,H+}(r) = \begin{cases} \dfrac{B_p(r - r_p)^4}{r} & r < r_p \\ 0 & r > r_p \end{cases}. \tag{16}$$

This is one of the most simple analytical function which was found to be effective in describing the repulsive part of the ionic potential involving proton, and which allowed the AVB parametrization to reproduce the DFT results.

Use of an Auxiliary Two-State Hamiltonian and Construction of the Nondiagonal Matrix Elements

The molecular valence forms formulated for the description of the quantum region can be equally well used to construct the Hamiltonians of the separated constituents of the region. These Hamiltonians should reproduce potential energy surfaces as well as the electronic structure of the isolated molecules. It will also be shown that within the two-state AVB model one can approximate results of more advanced quantum-chemical calculations in the presence of the external electrostatic field. This provides a possibility to use the two-state models to parametrize canonical structures of molecules as well as the off-diagonal elements of the Hamiltonian matrix using DFT and ab initio calculations. Let us consider well-defined examples. In particular the water molecule, regardless whether it is part of the active site or it is the molecule in the gas phase, can be represented by a mixture of the covalent and ionic structures: HO — H and OH^-H^+. These two structures can describe the geometrical and electrostatic properties in equilibrium as well as the radical or the ionic dissociation process of the proton. In particular, the ionic dissociation leads to the OH^- group which can be parametrized to render microscopic properties of real hydroxyanion. A similar interpretation applies for the pair of structures H^+Im and H — Im^+. Im denotes a single structure which mimics properties of the neutral imidazole ring and the combination of both structures describes the protonated imidazole. All chemical bonds except the NH bond exhibit a mixed character. Next, the combination of the structures abbreviated as O = C and ^-O — C^+ gives the isolated substrate molecule, and the mixture of the structures ^-O — C^+OH^- and ^-O — C — OH describes the intermediate state during the hydrolysis process. Consider now a pair of valence structures describing a molecular fragment. We may think of the covalent and ionic forms of an isolated water molecule. The two-state AVB description of this molecule leads to the following eigenvalue problem:

$$\begin{pmatrix} H'_{11} - E^0 & H_{12} \\ H_{12} & H'_{22} - E^0 \end{pmatrix}\begin{pmatrix} c_1 \\ c_2 \end{pmatrix} = 0, \tag{17}$$

where H'_{11} and H'_{22} are the diagonal elements related to the covalent and ionic forms of the water molecule described by Eq. (8). The prime symbol denotes that the valence structure is limited to the given molecule extracted from the larger system. As mentioned above, in this case E^0 as the function of the atomic positions can be used to calculate the nondiagonal matrix elements:

$$H_{12} = H_{21} = \sqrt{(H'_{11} - E^0)(H'_{22} - E^0)}. \tag{18}$$

The parameters which appear in E^0 can directly be determined by fitting its analytical representation to the quantum-mechanical and experimental energy data. In particular, high-quality experimental data in the vapor state can be used to calibrate the parametrization. The diagonal matrix elements H'_{ii} do not have such a simple reference. However, an idea introduced by Warshel opens the way to an additional interpretation of the diagonal elements. Namely, in the presence of an environment, the electronic ground-state energy of the molecule is determined by the secular equation (17) with the

perturbed diagonal elements:

$$\begin{pmatrix} H'_{11} + \Delta H_{11} - E & H_{12} \\ H_{12} & H'_{22} + \Delta H_{22} - E \end{pmatrix} \begin{pmatrix} c_1 \\ c_2 \end{pmatrix} = 0, \tag{19}$$

where ΔH_{11} and ΔH_{22} represent interactions between the environment and the molecule frozen in its covalent or ionic form. In the case of the electrostatic interactions we assume:

$$\Delta H_{ii} = k \sum_{a \in \text{mol}} q_{a,i} V_a, \tag{20}$$

where $i = 1,2$, $q_{a,i}$ denote the atomic charges in the structure i of the molecule, and V_a is the electrostatic potential at the atom a of the molecule generated by the atoms of the environment,

$$V_a = \sum_{b \in \text{env}} \frac{q_b}{r_{ab}}. \tag{21}$$

Based on the model formulated above we will present three useful relations for further development of the AVB method.

Let $\mathbf{H}^{\text{tot}}$ denote the Hamiltonian matrix containing the diagonal perturbation (20). The energy eigenvalue E, which satisfies (19) and corresponds to the normalized eigenvector $\{c_i\}$, can be expressed as

$$E = \sum_{ij} H_{ij}^{\text{tot}} c_i c_j. \tag{22}$$

First, differentiating the last formula with respect to the coordinates of the atoms belonging to the environment we obtain an AVB version of the conventional, stationary Hellmann–Feynman forces (see Appendix 1):

$$\frac{\partial E}{\partial \mathbf{R}_C} = \sum_i \frac{\partial H_{ii}^{\text{tot}}}{\partial \mathbf{R}_C} c_i^2 = k \sum_{a \in Q} \frac{\partial V_a}{\partial \mathbf{R}_C} \sum_i q_{a,i} c_i^2, \tag{23}$$

which means that the electrostatic forces acting on the atoms of the environment can be calculated using the effective atomic charges in the molecule,

$$q_a = \sum_i q_{a,i} c_i^2. \tag{24}$$

Second, in the two-state AVB description of the unperturbed molecule the normalized coefficients c_1 and c_2 can be easily expressed by the elements of the Hamiltonian matrix (17) and the following relation between the effective atomic charges and the Hamiltonian matrix elements results from (24):

$$\frac{q_a - q_{a,1}}{q_{a,2} - q_a} = \frac{H'_{11} - E^0}{H'_{22} - E^0}, \tag{25}$$

for all atoms a in the molecule. The above expression will be used to reduce the freedom of the parametrization of the atomic charges characteristic for the VB structures $\{q_{i,a}\}$ as well as of the parametrization for the diagonal elements $\{H'_{ii}\}$. In particular we require that the effective atomic charges $\{q_a\}$ of the unperturbed molecular fragments be identical to ESP charges, computed using the DFT method and reproducing the molecular electrostatic potential, see [3, 40] for details. However, formula (25) defines only the relative positions of the diagonal element surfaces above the surface of the total ground-state energy. Coming then to the third relation, let us note that a finite electrostatic perturbation of the AVB eigensystem modifies its ground state energy as well as the valence state itself. The eigenvector represented by the coefficients $\{c_i\}$ and the effective charges $\{q_a\}$ vary under the perturbation. This is a nonlinear effect and can be described in terms of the molecular polarizability. The total energy E of a molecular system in an external uniform electrostatic field $\mathbf{K}$ can be expanded in the Taylor series:

$$E(\mathbf{K}) = E^0 - k\,\mathbf{d}\mathbf{K} - \tfrac{1}{2} k \mathbf{K} \hat{\alpha} \mathbf{K} + \cdots, \tag{26}$$

where $\mathbf{d}$ is the effective dipole moment resulting from the charge distribution $\{q_a\}$ in the unperturbed molecule and $\hat{\alpha}$ is the polarizability tensor. It can be calculated based on the two-state AVB model (see Appendix 1) that

$$\hat{\alpha} = \frac{2kc_1^2 c_2^2 \Delta\mathbf{d}\,\Delta\mathbf{d}^T}{H'_{11} - H'_{22} - 2E^0}, \tag{27}$$

where $\Delta\mathbf{d}$ denotes the difference between the dipole moments resulting from the charge distributions $\{q_{a,i}\}$ and $\{q_{a,j}\}$. The coefficients c_1 and c_2 are the components of the normalized eigenvector of the unperturbed Hamiltonian. In this way the

polarizability of the two-state system provides an additional information imposing constraints on the parametrization of H'_{11} and H'_{22}.

Nondiagonal Elements of the Full AVB Hamiltonian Matrix and Coupling between the Quantum and Classical Regions

The model of the perturbed two-state Hamiltonian matrix (19) implies the method for calculation of the nondiagonal elements of the many-state AVB Hamiltonian for the quantum region, as well as the coupling mechanism between the quantum and classical regions. The nondiagonal elements of the Hamiltonian matrix are assumed to be nonzero quantities only for those pairs of the valence structures which differ in the description of one chemical bond. For example, in the set of eight structures listed above for the quantum region of PLA_2 the structure ψ_1 is coupled with the structures ψ_2 and ψ_4. To calculate the element H_{ij} a molecular fragment discriminating the structures ψ_i and ψ_j is extracted from the system. For this fragment we calculate the energies H'_{ii} and H'_{jj} from the formulas used previously to calculate the elements H_{ii} and H_{jj}, with the exception of all elementary potentials which involve atoms not included in the fragment. Then the additional energy term, E^0_{ij}, is calculated. It represents the energy of the selected fragment in the ground valence state. This energy is also a sum of analytical elementary potentials of the form (8), with its own set of parameters. Finally, the value of H_{ij} is calculated using the formula (18), and it is used as the approximation of the nondiagonal multistate Hamiltonian matrix element.

The above procedure can be illustrated by calculation of the H_{12} or H_{14} elements appearing in the eight-state Hamiltonian of the PLA_2 quantum region. In this case H'_{11} is the energy of the covalent structure (HO — H), H'_{22} and H'_{44} are identical and represent the energy of the ionic structure (HO^-H^+), and similarly E^0_{12} and E^0_{14} are equivalent and denote the real ground-state energy of the water molecule. In a simplest approach proposed by Warshel, the expressions for H'_{ii}, H'_{jj}, and E^0_{ij} are restricted to the potentials involving only the pair of atoms forming the considered ionic or covalent bond. This approach could also be applied in our computer implementation of the AVB method, but it would complicate parametrization of the electrostatic properties.

Since the whole molecular system in our model is described with a combination of the AVB and PF methods, some interaction potentials of the quantum region can be omitted in the terms H'_{ii}, H'_{jj}, and E^0_{ij} appearing in expressions (8) and (18). This refers to those potentials, which are identical for all valence structures as well as for the ground-state energy. These energy terms are additive with respect to the eigenvalues of the AVB system (6) and can be calculated separately using the PF analytical approximation. In our parametrization we use the above approach for the bonding interactions inside the imidazole ring and selected bonding interactions in the substrate molecule.

The diagonal perturbation of the Hamiltonian matrix is also used to describe the influence of the classical region on the multidimensional AVB Hamiltonian of the quantum region. The ground valence state energy of the perturbed quantum region is calculated from the following eigensystem:

$$\det(\mathbf{H}_Q + \Delta\mathbf{H}_{QC} - \mathbf{I}E) = 0. \qquad (28)$$

$\mathbf{H}_Q$ denotes the AVB Hamiltonian of the separated quantum region and $\Delta\mathbf{H}_{QC}$ is the diagonal interaction matrix between the quantum and classical regions, analogous to the interaction matrix defined in the two-state Hamiltonian; see Eq. (19). The elements of the interaction matrix are approximated as a sum of the elementary interatomic potentials. The potentials describing chemical interactions between two regions (bonds, angles, etc.), as well as the nonbonding interactions except for the electrostatic terms, are assumed to be equivalent for all VB structures of the quantum region. These terms influence the energy eigenvalues in an additive way and can be calculated separately. The electrostatic interactions must be included explicitly in Eq. (28) since the valence structures differ in their distribution of the atomic charges. The energy of the electrostatic interactions between the VB structures and the classical region is calculated using the formula (21). Finally, the total potential energy surface for the classical atomic motions, in both the classical and quantum regions, is calculated as the sum:

$$E^{\text{tot}} = E^{\text{AVB}} + V^{\text{PF}}, \qquad (29)$$

where E^{AVB} denotes the ground energy eigenvalue of the system (28), and V^{PF} denotes all potential energy function terms mentioned above including atomic interactions in the classical region and the additive energy terms not included in the AVB Hamiltonian. This approach allows for some improvements of the MD algorithm. The forces acting on the atoms in the classical region do not require differentiation of the E^{AVB} energy using the finite difference method with a multiple evaluation of the Hamiltonian matrix and its eigenstates but can be computed directly at the given atomic positions using formula (23), which gives:

$$\mathbf{F}_{b\in C} = -\frac{\partial V^{PF}}{\partial \mathbf{R}_b} + kq_b \sum_{a\in Q} \frac{\mathbf{R}_{ba} q_a}{R_{ba}^3},$$
$$\mathbf{R}_{ba} = \mathbf{R}_b - \mathbf{R}_a. \qquad (30)$$

Model Molecular Systems and Quantum Mechanical Calculations

Most of the calculations were performed using the DFT method with the DMOL Biosym package. The local electron density Hedin–Lundqvist/Janak–Morruzi–Williams functional [34] and the double numerical basis set of atomic orbitals plus polarization functions (DNP) were used. The total electron spin was restricted to 0 except for products of radical dissociation reactions. The calculations were performed for a large number of molecular conformations which covered most important configurational regions in the modeled biochemical processes. Although the local density approximation (LDA) overestimates the hydrogen bond energies, it provides satisfactory results for the geometry optimization as well as for relative total energies. The LDA approximation also gives atomic ESP charges which are very close to the charges calculated using conventional ab initio MP2 methods with a comparable basis set [40]. For DFT studies on hydrogen-bonded complexes see, e.g. [35, 36]. Our procedure for fitting the ESP charges to the molecular electrostatic potential based on the DFT calculations [40] is very similar to that one implemented in the GAUSSIAN program [37, 38].

The model systems for the enzyme active site are the water molecule, imidazole ring (Im), and a simple ester, methyl acetate (CH_3COOCH_3, or in some calculations methyl propionate, $C_2H_5COOCH_3$). A model complex comprising these molecules is presented in Figure 5. The H5 proton is transferred between the water molecule and imidazole. The remaining hydroxyanion attacks the carbonyl carbon (C2) of the substrate and the intermediate molecular structure, $CH_3C(OH)OOCH_3^-$, is formed. The geometries of all isolated molecules were optimized. Next the conformational and electrostatic properties as well as dissociation processes of the water molecule, the protonated imidazole, the initial substrate and the intermediate product of the nucleophilic attack were studied. Finally the complexes imidazole–water, water–ester, and imidazole–water–ester were studied.

WATER MOLECULE AND ITS DISSOCIATION

The DFT radical and ionic dissociation energies for the water molecule were calculated as the differences between the total energies of the dissociation products (OH and H, or OH^- and H^+, respectively) and the energy of the water molecule at its optimal geometry. The resulting values are 134.5 for the radical and 386 kcal/mol for ionic dissociation process. The corresponding experi-

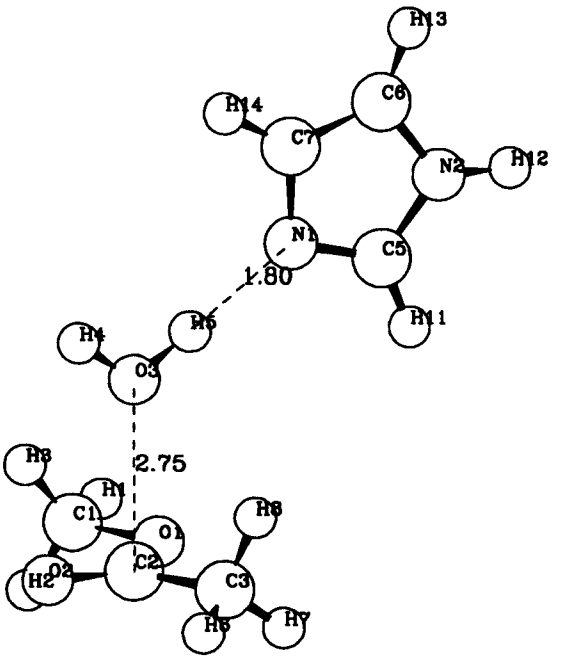

FIGURE 5. Model of the enzymatic complex used for the DFT calculations.

mental enthalpies, corrected for the zero-point vibrational energies and the temperature-depending kinetic terms (about +8 kcal/mol), are 126 and 398 kcal/mol, respectively. The energy curve for the hydrogen dissociation, obtained at the fixed second OH bond length and the HOH angle, can be very well approximated by a Morse function up to the distance of 1.8 Å. Beyond this distance separation of the spin density between OH and H is observed, and the close shell calculations are no longer adequate. The optimized Morse amplitude is 136 kcal/mol (close to the calculated radical dissociation), equilibrium distance is 0.985 Å, and the equilibrium force constant is 1108 kcal/mol $Å^{-2}$. The changes of the ESP charges during the dissociation are presented in Figure 6. This behavior can be reproduced in the two-state AVB model of the molecule using the approach presented in above. The effective polarizability obtained in the assumed AVB parametrization of the water molecule is close to the value derived from the DFT calculations for the water molecule in external electrostatic field (mean polarizability 1.35 $Å^3$ in the plane of the molecule, experimental value is approximately the same). The potential of the HOH angle was parametrized using several sets of DFT energy data obtained for angular deformations of the molecule at one OH bond fixed at its optimal value and the second varied in the range 0.8–1.8 Å.

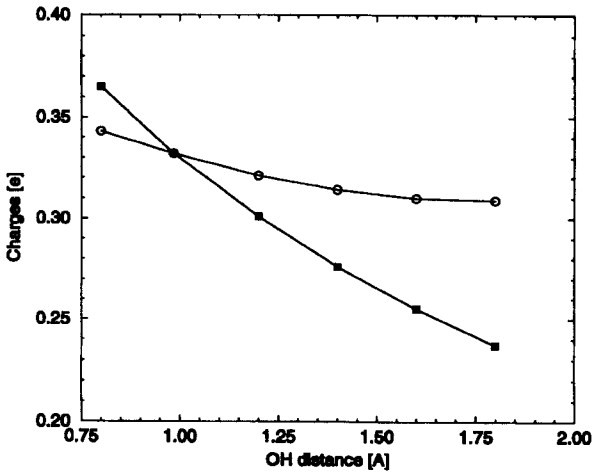

FIGURE 6. ESP charges at the hydrogens in water during the radical dissociation process. Squares and circles refer to the dissociated hydrogen and the fixed hydrogen, respectively. The sum of the ESP charges in the molecule is 0.

NEUTRAL AND PROTONATED IMIDAZOLE

The DFT energy of the proton bonding to imidazole is −223 kcal/mol. The experimental proton affinity is −221 kcal/mol and the corrections for zero-point vibrational energy and kinetic terms give a lower value, −229 kcal/mol. The dissociation of the hydrogen atom from the protonated imidazole *in vacuo* leads, like in the case of the water molecule, to radical products. The DFT energy change in this process is 133 kcal/mol, while the experimental value is about 118 kcal/mol (based on ionic dissociation energy of protonated imidazole, −229 kcal/mol, electron ionization energy of neutral imidazole, −202.5 kcal/mol, and ionization energy of hydrogen, 313.4 kcal/mol). The DFT energy data for the protonated imidazole at its optimal geometry and with N1H5 distance varied within the range 0.8–2.0 Å have been used to fit the Morse potential. The optimum N1H5 length is 1.029 Å, the Morse amplitude 135.5 kcal/mol, and the force constant at the equilibrium distance 963 kcal/mol $Å^{-2}$. The relative energies for angular displacements of H5 hydrogen with respect to the ring in the protonated imidazole were also calculated. First, the potential energies for planar deformations of the angles C5N1H5 and C7N1H5 were fitted based on the DFT calculations at various N1H5 distances. The next set of calculations was performed for displacements of H5 out of the ring's plane. These data were used to calculate the force constant of the harmonic potential for the H5C5C7N1 improper dihedral angle. Use of this angle for the description of the out-of-plane motion of H5 depends on the way the imidazole ring configuration is defined in the classical PF. Note, that all the conformational potentials of the imidazole ring, except the potentials related with the H5 in the protonated form, are calculated in the PF part of the QCMD/AVB algorithm.

The ESP charges of the neutral and protonated imidazole ring are presented in Table I. In the case of the imidazole, as well as in the case of the ester, two approaches for the charge fitting should be distinguished. In the first model the charges are optimized for all atoms (*all atom* model); in the second one, applied in the current AVB parametrization, hydrogens connected to the carbon atoms are neglected (*united atom* model). We found that the ESP charges in these models are quite different.

TABLE I

ESP charges calculated within the *united atom* model for water, imidazole and their complex (O3N1 = 2.8 Å, O3H5 = 1.0 Å), as well as for hydroxyanion, protonated imidazole, and their complex (O3N1 = 2.8 Å, H5N1 = 1.0 Å).

	Separate molecules		Molecules in the complexes	
Atom	H_2O, Im	OH^-, ImH^+	H_2OIm	OH^-ImH^+
H4	0.339	0.027	−0.370	0.261
O3	−0.678	−1.027	−0.818	−0.962
H5	0.339	0.612	0.400	0.548
N1	−0.537	−0.875	−0.575	−0.731
C5	0.436	0.755	0.554	0.681
N2	−0.691	−0.875	−0.829	−0.888
H12	0.463	0.612	0.507	0.550
C6	0.144	0.386	0.244	0.328
C7	0.184	0.386	0.137	0.212

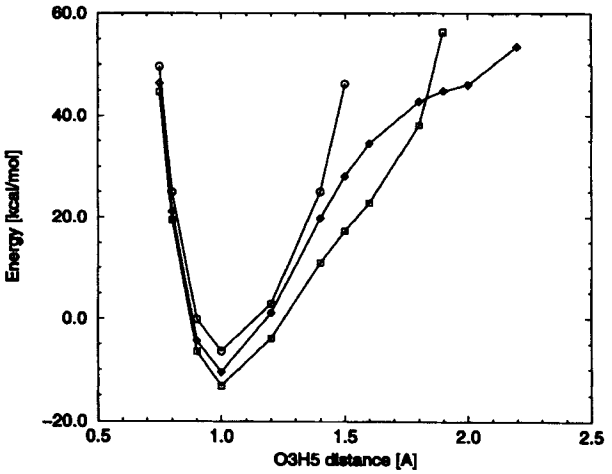

FIGURE 7. DFT binding energy of the water–imidazole complex plotted with respect to the O3H5 distance at three values of the O3N1 distance: 2.4 (circles), 2.8 (squares), and 3.2 Å (diamonds).

Polarizability of the neutral and protonated imidazole was derived from the DFT calculations in external electrostatic fields. The polarizability of neutral imidazole is 8.5 ± 0.5 $Å^3$ in the plane of the molecule and 4.2 $Å^3$ in the perpendicular direction. Polarizability of protonated imidazole in the plane of molecule is 7.3 ± 0.5 $Å^3$. The molecular polarizability can be approximately decomposed into diatomic contributions by monitoring changes of the ESP charges. This procedure gives in the *united atom* model the polarizability of 2 $Å^3$ for the N1H5 bond.

PROTON TRANSFER IN THE WATER–IMIDAZOLE COMPLEX

In the model complex of water and imidazole both molecules are placed in the same plane and form the linear hydrogen bond involving the O3, H5, and N1 atoms located along the bisector of the C5N1C7 angle in the imidazole ring. The optimized geometries of the individual molecules were used. The energy of the complex was computed for various values of the O3H5 and O3N1 distances (see Fig. 7). The binding energy has its lowest value, −13 kcal/mol, for O3N1 = 2.80 Å and O3H5 = 1.00 Å. The MP2/6-31G(d) calculations performed by us for the same system give the binding energy −7 kcal/mol at the optimal O3N1 distance 3 Å. Table I contains the ESP charges of the water–imidazole complex. Two geometries of the complex were studied: the optimal one and with the H5 proton transferred to N1 nitrogen with fixed positions of the other atoms. For comparison the ESP charges of the separated molecules, water, neutral imidazole, OH^- and protonated imidazole, are shown in the same table.

MODEL ESTER AND ITS INTERACTION WITH THE WATER MOLECULE

The methyl acetate and the methyl propionate molecules were used in the DFT calculations to model the fragment of the substrate involving the ester bond hydrolyzed by PLA_2. The molecule of methyl acetate was optimized (see Table II) resulting in an almost coplanar position of all heavy atoms. The molecule of methyl propionate was obtained from the previous one by optimization of

TABLE II

Optimized distances and planar angles in methyl acetate and methyl propionate.[a]

ABC seq.[b]	BC (Å)	ABC (deg)
O2C2	1.218	—
O2C2C3	1.483	125.7
C2C3C4	1.540	98.9
O2C2O1	1.351	122.7
C2O1C1	1.427	113.0

[a]All heavy atoms are located in the plane of the molecule.
[b]ABC denote the sequence of the atom names.

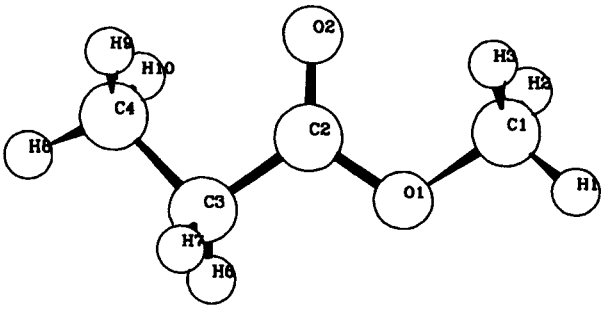

FIGURE 8. Methyl propionate molecule.

the position of the additional methyl group C4 (see Fig. 8). Then the studies of conformational, electrostatic, and intermolecular interaction properties of the ester molecule were performed. Table III presents calculations of the ESP charges for the methyl acetate molecule *in vacuo* and in the presence of a single point charge ($+1e$) located on the axis of the C2O2 bond, 2.5 Å apart from the O2 oxygen and modeling the influence of the screened calcium cation in the enzyme active site. The interactions between the ester and the water molecule were studied using the optimized geometries of the separated molecules. The water molecule was placed in a plane perpendicular to the plane of the ester molecule. The symmetry axis of the water molecule was crossing the ester at the positions of the C2, C3, O1, and O2 atoms. The water oxygen, O3, was oriented toward the ester. The relative energies of the complex at various distances between the molecules are shown in Figure 9. The

TABLE III

ESP charges calculated in the *united atom* model for methyl acetate *in vacuo*, in the presence of a point charge (+1) Located 2.5 Å apart from the O2 atom and in the presence of the water molecule located 2.5 Å apart from the C2 atom (see the text).

Atom	Vacuo	Point charge	Water
C1	0.274	0.313	0.229
O1	−0.392	−0.339	−0.338
C2	0.536	0.615	0.479
O2	−0.485	−0.741	−0.444
C3	0.067	0.153	0.051
O3	—	—	−0.689
H4	—	—	0.360
H5	—	—	0.352

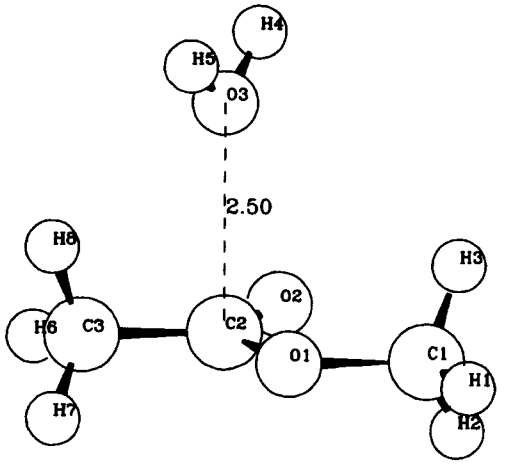

FIGURE 9. A typical configuration of the complex between the model ester and water molecules.

ESP charges for the water–ester complex were also fitted at various positions of the water molecule. Selected results obtained in the presence of the water molecule placed at the optimal distance from the C2 carbon (2.5 Å, compare Figure 10) are shown in Table III.

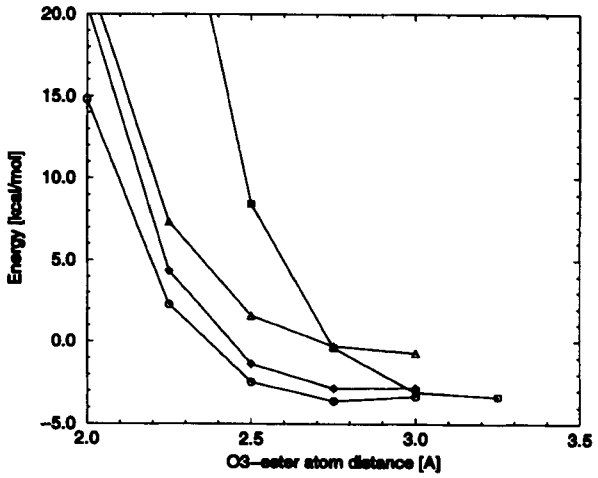

FIGURE 10. DFT energy profiles describing the interactions between the methyl acetate and the water molecule. The circles, squares, diamonds, and triangles refer to the data obtained at various distances between the water oxygen atom, O3, and the C2, C3, O1, O2 atoms of the ester molecule, respectively. See the text for description of the geometries.

HYDROXYESTER ANION—THE MODEL SYSTEM FOR THE TETRAHEDRAL INTERMEDIATE STATE

The nucleophilic substitution of the OH^- group at the carbonyl carbon of the ester bond leads to hydroxyester anion. The molecules $CH_3C(OH)OOCH_3^-$ and $C_2H_5C(OH)OOCH_3^-$ were chosen as model systems for the real intermediate state. The geometry of the first molecule was fully optimized; the second molecule was obtained by addition of the methyl group C4 and optimization of its position (see Fig. 11 and Table IV). The conformational and electrostatic properties of these molecules were studied. In particular, two energy profiles describing the C2O3 bond were generated. The first one was obtained by moving OH^- away from the model tetrahedral intermediate state, and the second one by moving OH^- toward the neutral model ester with the planar configuration of the carbonyl carbon (in the last case the same relative orientation of ester and the O3H4 group was used as in the calculations of the water molecule attacking the ester; compare Fig. 9). During the dissociation or addition processes, presented in Figure 12, the geometries of the objects were fixed except for the distance between the OH^- and the carbonyl carbon. Table V presents selected results of the ESP charge calculations for hydroxyanion and the ester molecule in both processes.

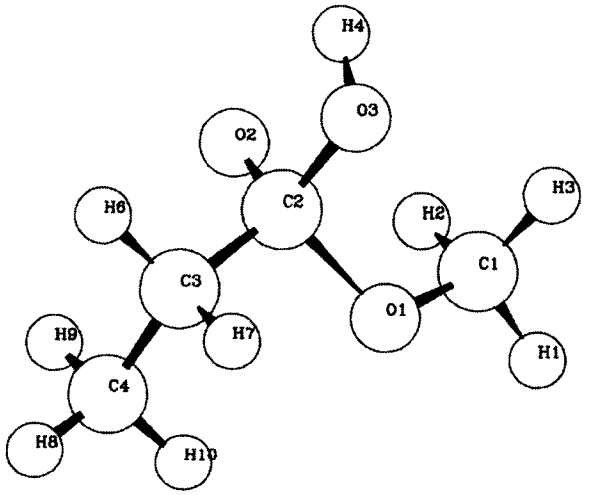

FIGURE 11. Optimized geometry of the $C_2H_5C(OH)OOCH_3^-$ molecule resulting from the nucleophilic attack of the hydroxyanion on the methyl propionate.

TABLE IV
Optimized distances, planar angles, and torsions in hydroxyester anion.[a]

ABCD seq.	CD (Å)	BCD (deg)	ABCD (deg)
H4O3	0.989	—	—
H4O3C2	1.490	96.2	—
H4O3C2O2	1.289	110.7	2.0
H4O3C2C3	1.523	106.1	−127.0
H4O3C2O1	1.496	104.1	126.0
O2C2O1C1	1.395	110.9	42.0
O2C2C3C4	1.539	108.8	60.0

[a]ABCD denotes the sequence of the atom names.

Another important set of DFT energy data was generated by manipulation of the atomic configuration at the C2 carbon at various C2O3 distances. In the AVB parametrization of the isolated hydroxy-ester anion molecule, the optimal, tetrahedral geometry of the C2 carbon results from the energetic "compromise" of mainly three factors acting against each other. The first one comprises planar angle potentials (O1C2O3, O2C2O3, and C3C2O3), which impose the tetragonal configuration configuration at C2 but vanish at longer C2O3 distance. The second one is the potential of the

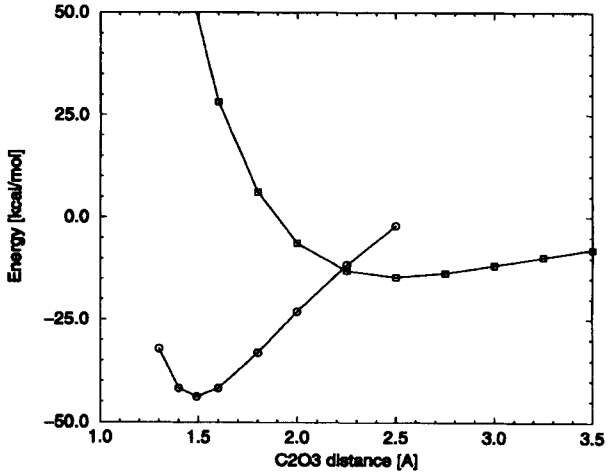

FIGURE 12. The DFT energy profiles for the dissociation of the hydroxyanion leaving the $CH_3C(OH)OOCH_3^-$ molecule in fixed, tetrahedral configuration (circles), and the addition of the hydroxyanion to the CH_3COOCH_3 molecule fixed at its optimal, planar geometry (squares). The asymptotic values of these profiles are 38.5 and 0 kcal / mol, respectively, on a relative energy scale.

TABLE V

ESP charges of $CH_3C(OH)OOCH_3^-$ molecule, which mimics the tetrahedral transition state, at optimal (1.49 Å) and stretched (2.25 Å) C2O3 bond length, and charges in the planar ester in complex with OH^- at squeezed (2.25 Å) and optimal (2.5 Å) C2O3 distance.

	Tetrahedral configuration		Planar configuration	
Atom	Optimal	Stretched	Squeezed	Optimal
C1	−0.011	0.041	0.086	0.100
O1	−0.431	−0.392	−0.269	−0.268
C2	0.915	0.789	0.402	0.406
O2	−0.804	−0.647	−0.449	−0.441
C3	−0.248	−0.167	−0.075	−0.058
O3	−0.687	−0.833	−0.862	−0.880
H4	0.266	0.210	0.167	0.141

improper dihedral angle, C2O1C3O2, which acts toward the coplanar position of the C2, O1, C3, and O2 atoms. It does not depend on the C2O3 distance and is responsible for the planar conformation of the ester achieved after the separation of hydroxyanion. Finally, the potential of C2O3 bond prevents hydroxyanion from being "pushed out" from the C2 carbon by the influence of the angular energy contributions.

AVB Parameters

In this section we present a complete set of AVB parameters applied to the quantum region of phospholipase A_2. The atoms belonging to the quantum region are identified by the names used in the DFT calculations. In the parametrization of the nonbonding valence interactions, described by the potentials (14) and (16), we use an additional set of codes denoting the atomic "valence type." These codes as well as values of the atomic charges are assigned to the atoms separately in each molecular fragment used in the valence structures (see the valence structures in the third section). The list of electrostatic and valence interactions within a structure is determined similarly to the PF rules, namely, the atoms interact if they are separated or connected by a chain of three or more chemical bonds. The exception is the neutral imidazole and the covalent state of the protonated imidazole inside which the nonbonded interactions are eliminated for any pair of the atoms. Assignment of the atomic valence types and charges in the subsequent molecular fragments is presented in Table VI, VII, VIII, and IX. Note that the values of the atomic charges do not correspond in detail to the purely ionic or covalent schemes. As already discussed the charges should reproduce the effective electrostatic properties of the given system. In particular, the charges in the hydroxyanion or neutral imidazole come directly from the ESP calculations, while the charges in other fragments ensure that the ESP results are reproduced in the two-state AVB Hamiltonian of the separated water, protonated imidazole, ester, or hydroxyester anion. Note also that for molecules containing carbons the *united atom* model is used with the proper set of charges. Note finally that the valence types and atomic charges must be also assigned for the ester molecule and hydroxyester anion in their ground states. This is because of interatomic nonbonding interactions within these molecules which are in-

TABLE VI

Atomic charges and valence types in the covalent and ionic states of the water molecule and the effective charges in its ground state.

	HO — H		OH^-H^+		Ground state
Atom	Type	q	Type	q	q
H4	H	0.499	H	0.027	0.339
O3	OW	−0.499	OW −	−1.027	−0.678
H5	H	0.000	H +	1.000	0.339

TABLE VII

Atomic charges and valence types in the covalent and ionic states of the protonated imidazole and the effective charges in its ground state.

	Im^+— H		Im H^+		Ground state
Atom	Type	q	Type	q	q
H5	H	0.377	H +	1.000	0.612
N1	NR	−1.079	NR	−0.537	−0.875
C5	CR	0.948	CR	0.436	0.755
N2	NR	−0.986	NR	−0.691	−0.875
H12	H	0.702	H	0.463	0.612
C6	CR	0.532	CR	0.144	0.386
C7	CR	0.506	CR	0.184	0.386

TABLE VIII
Atomic charges and valence types in covalent, ionic, and ground states of the ester molecule.

	O = C		$^{-}$O — C^{+}		Ground state	
Atom	Type	q	Type	q	Type	q
C1	CH	0.397	CH	0.132	CH	0.274
O1	OE	−0.392	OE	−0.392	OE	−0.392
C2	C	0.000	C	1.155	C	0.536
O2	O	−0.209	O	−0.804	O	−0.485
C3	CH	0.204	CH	−0.091	CH	0.067
C4	CH	0.000	CH	0.000	CH	0.000

cluded in the potential energy surface. Parameters for nonbonding valence interactions, depending on the valence types, are presented in Tables X and XI.

In the case of "dissociable" bonds represented by their ionic and covalent forms, the parametrization of the valence and electrostatic interactions in the ionic form is strictly connected with the parametrization of the Morse potential of the covalent form. In this case the two-state Hamiltonian (17) is used. The potential terms representing the ground energy, E_{ij}^{0}, were first fitted directly to the DFT potential surface for the bond dissociation or to analogous experimental data. Next the parameters in the H'_{ii} and H'_{jj} matrix elements were determined with the help of the Eqs. (25) and (27). The parameters of the remaining nonbonding valence interactions were computed by fitting the numerically solved eigenvalue of a proper Hamiltonian matrix to the DFT energy curves for the molecular complexes. In the case of the water–imidazole complex the MP2 data were rather used in order to establish parameters of the nonbonding interactions between water and imidazole. We also tried to reproduce the redistribution of the ESP charges during formation of the complexes. These fits were done for the separated water–imidazole and water–ester complexes.

The constant energy terms contributing to the energies of the valence structures (diagonal elements of the Hamiltonian matrix) were decomposed into the energies assigned to the individual covalently bonded molecular fragments (see Table XII). In order to calculate the total constant energy V^{0} of a given valence structure, one has to add the partial energy terms V_{m}^{0} of the molecular fragments found in this structure. In some of the cases listed in Table XII a method of a "charge adjustment" is reported. This method refers to the two-state Hamiltonian parametrization, in which the energy surfaces related with the diagonal elements are calibrated based on a given ground-state energy and relations assuring the proper charge distribution in the ground state (usually this procedure was applied using the optimal geometries of the modeled systems and along the trajectories of the bond dissociations). The ground-state energies, E^{0} appearing in these Hamiltonians have their

TABLE IX
Atomic charges and valence types in the covalent, ionic, and ground states of the hydroxyester anion.

	$^{-}$O — C — OH		$^{-}$O — C^{+} OH^{-}		Ground state	
Atom	Type	q	Type	q	Type	q
C1	CH	−0.064	CH	0.132	CH	−0.011
O1	OE	−0.445	OE	−0.392	OE	−0.431
C2	C	0.826	C	1.155	C	0.915
O2	O	−0.804	O	−0.804	O	−0.804
O3	OA	−0.561	OW −	−1.027	OA	−0.687
H4	H	0.354	H	0.027	H	0.266
C3	CH	−0.306	CH	−0.091	CH	−0.248
C4	CH	0.000	CH	0.000	CH	0.000

TABLE X
Parameters for nonbonding valence interactions defined for the pairs of the specified atomic valence types.[a]

Atom 1	Atom 2	B (kcal / mol Å^6)	b (Å^{-1})	C (kcal / mol Å^6)
H	H	6000	2.300	51
H	C*	19000	1.800	188
H	NR	13000	2.100	130
H	OW −	11350	2.200	136
H	O*	10000	2.200	106
C	OW*	10540	1.499	334
CH	CH	85500	1.000	4173
CH	OW*	71760	0.973	3778
CH	O*	48450	1.000	4447
CR	OA	79000	1.630	392
CR	OW*	79000	1.630	392
NR	OA	70000	1.680	751
NR	OW*	70000	1.680	751
O	OW*	15680	1.075	508
OE	OW*	90920	2.307	345
*	*	Calculated in the PF part of the algorithm		

[a]Asterisk denotes any string of characters in the given position (in particular an empty string). The names with asterisks have lower priority in the list than the explicit names.

own constant energy terms V^0 listed in Table XIII. They were normalized to set the AVB energy level to zero in the case when the system consists of noninteracting, separated compounds: water, imidazole, and ester at their optimal geometries. For this reason the constant terms, V^0, for the ester molecule and hydroxyester anion, include a contribution which cancels with the sum of the elementary potentials related to internal conformational and nonbonding interactions (calibration of the ground-state energy at the optimal geometry).

TABLE XI
Parameters for nonbonding valence interactions between the proton (H^+) and other atoms.[a]

Atom	B_p (kcal / mol Å^{-3})	r_p (Å)
H	1.000	3.32
C*	2.000	2.00
NR	1.450	3.40
OW −	1.509	3.57
OA	1.509	3.57
O*	2.000	2.00

[a]Atoms are indicated by their valence types as in Table X.

TABLE XII
Constant energy terms for the molecular Fragments existing in the valence structures.

Molecule	V_m^0	Evaluation method (see text)
OH^-	390.0	Ionic dissociation energy of water
H^+	0.0	—
Im	0.0	—
HO — H	38.0	Charge adjustment for H_2O
Im^+— H	−141.8	Charge adjustment for ImH^+
O = C	38.6	Charge adjustment for ester
$^-$O — C^+	50.4	Charge adjustment for ester
$^-$O — C — OH	468.5	Charge adjustment for hydroxyester plus V_m^0 of OH^-

The analytical forms of the bonding potentials forming the "mechanical" part of the AVB Hamiltonian are described in the fourth section. In Table XIV the parameters of the Morse potentials for the bonds in the covalent states (used in diagonal elements of the Hamiltonian matrices) and ground states (used in the E^0 potential surfaces, in the two-state Hamiltonian models) are presented. Usually the covalent and ground-state parameters are different and derived in the previously described parametrization procedure. Tables XV and XVI contain the parameters of the bond-dependent and bond-independent angular potentials, respectively. The first set is used for the angles which are

TABLE XIII
Constant energy terms and the total ground-state energies for the molecules at their optimal geometries.

Molecule	V^0	Evaluation method E^0	for V^0
H_2O	0.0	0.0	—
ImH^+	−229.0	−229.0	Proton affinity of imidazole
Ester	23.2	0.0	Ground-state calibration
Hydroxyester	435.6	390.0	Ground-state calibration plus V_m^0 of OH^-

TABLE XIV
Parameters of the Morse potentials.

Bond	D_0 (kcal / mol)	a (Å^{-1})	r_0 (Å)
Water			
O3H5^{cov}	88.0	2.537	0.985
O3H5^{gr}	126.0	2.141	0.985
Protonated imidazole			
N1H5^{cov}	30.8	3.000	1.029
N1H5^{gr}	118.0	2.086	1.029
Covalent (C = O) and ground state of ester			
C2O2	180.5	2.251	1.218
C2O1	87.5	2.263	1.351
C2C3	92.3	1.953	1.484
Ionic state of ester ($^-$O — C$^+$)			
C2O2	122.6	2.198	1.293
C2O1	87.5	2.263	1.351
C2C3	92.3	1.953	1.484
Covalent ($^-$O — C — OH) and ground state of hydroxyester			
C2O2	122.6	2.198	1.293
C2O1	41.8	2.183	1.493
C2C3	79.5	1.913	1.526
C2O3^{cov}	26.6	1.880	1.730
C2O3^{gr}	33.4	2.389	1.488

adjacent to the dissociable bonds. In the current parametrization, the same set of parameters is used in both the covalent states and the ground energy states, although some more accurate models were tested to relate the parametrization of the angular distorsions with the charge redistribution within the two-state Hamiltonians. In Tables XVII and XVIII the parameters of the torsional and out-of-plane potentials are listed. These potentials are bond-independent except for the potential describing the motion of the H5 proton out of the ring plane in the protonated imidazole.

TABLE XV
Parameters of the planar angle potentials with the bond-dependent amplitudes.

Angle	A_0 (kcal / mol Å^{-1})	a (Å^{-1})	α_0 (deg)
Angles in water depending on the O3H5 distance			
H4O3H5	230.0	1.410	104.5
Angles in protonated imidazole depending on the N1H5 distance			
C5N1H5	151.0	1.165	126.0
C7N1H5	151.0	1.165	126.0
Angles in covalent and ground state of hydroxyester depending on the C2O3 distance			
O2C2O3	773.0	1.657	122.5
O1C2O3	10975.0	3.210	108.2
C3C2O3	46736.0	4.346	112.6
C2O3H3	393.0	1.657	109.1

TABLE XVI
Parameters of the torsional angle potentials (constant amplitudes).

Angle	A_0 (kcal / mol)	α_0 (deg)
Covalent, ionic, and ground state of ester		
O2C2O1	112.9	122.7
C2O1C1	110.4	116.3
O2C2C3	86.7	125.7
C2C3C4	113.9	110.7
O1C2C3	85.5	111.5
Covalent and ground state of hydroxyester anion		
O2C2O1	101.6	112.7
C2O1C1	110.4	116.3
O2C2C3	90.6	116.8
C2C3C4	113.9	110.7
O1C2C3	103.2	102.3

AVB Potential Energy Profiles for the Quantum Region and QCMD Simulations

The AVB ground-state energies for the active site and its components at selected geometries *in vacuo* are presented in Table XIX. The initial geometry of the complex (configuration 1) is based on the optimized water, imidazole, and methyl propionate molecules. The molecules were arranged as presented in Figure 5 (O3C2 = 2.75, O3N1 = 2.8, O3H5 = 1 Å). Configuration 2 was obtained by shifting the proton to the imidazole (H5N1 = 1 Å). Finally, configuration 3 was generated by shifting

TABLE XVII
Parameters of the torsional angle potentials (constant amplitudes).

Angle	A_0 (kcal / mol)	n	θ_0 (deg)
Covalent, ionic, and ground state of ester			
O2C2O1C1	6.8	2	0.0
O2C2C3C4	1.2	1	0.0
Covalent and ground state of hydroxyester			
O2C2O1C1	−1.5	3	0.0
O2C2C3C4	−2.0	3	0.0

TABLE XVIII
Parameters of the angular out-of-plane potentials.

Angle	Structure	A_0 (kcal / mol deg^{-2})	a (Å^{-1})	δ_0 (deg)
N1C7C5H5[a]	cov. and gr. st. of ImH$^+$	0.106	1.1653	0.0
C2O1C3O2	ground st. of ester	0.0457	—	0.0
C2O1C3O2	covalent st. of ester	0.0486	—	0.0
C2O1C3O2	ground st. of hydroxyester	0.0296	—	0.0

[a]Amplitude A_0 is given in kcal / mol deg^{-2} Å^{-1}, effective amplitude depends on the N1H5 distance.

TABLE XIX
AVB ground-state energies of the active site model and its components *in vacuo*.[a]

Complex	1	2	3
Ester–water–Im	−10.0	37.3	28.8
Water–Im	−6.2	40.6	—
Ester–water	−3.9	—	—

[a]See the text for description of configurations 1, 2, and 3. Energy in kcal / mol. The zero energy corresponds to the separated water, imidazole and ester molecules.

the hydroxyanion (kept in complex with the protonated imidazole ring) toward the ester molecule (O3C2 = 1.5 Å). At the same time the planar geometry of ester was modified to the optimal tetrahedral configuration of the hydroxyester anion. The AVB energy profile for the proton transfer in the model complex *in vacuo* (e.g., transformation between configurations 1 and 2) is shown in Figure 13. The similar profile was also calculated for the complex polarized by the point charge (+2) placed on the axis of the ester carbonyl bond, 2.5 Å apart from the O2 atom. In the last case a bistable potential curve appears. Figure 14 presents the energy profiles for the nucleophilic attack in the model complex *in vacuo* and in the presence of the (+2) point charge. Two hypothetical paths are considered. On the first one [the profiles (a) in the figure] the proton is bonded to the water molecule and the water–imidazole complex is moved to the planar ester. On the second path [profile (b)] the proton is bonded to the imidazole molecule and the hydroxyanion–imidazole complex is moved to the ester with the latter kept in the tetrahedral configuration.

The influence of the protein environment on the AVB ground-state energy surface for the active site is complex and varies in time. In the QCMD/AVB simulations of PLA_2 the AVB and PF potential energy surfaces are used to generate the forces for the classical motions of all the atoms in the enzyme–substrate complex (Fig. 1). Dynamics of the H5 proton is described by the time-dependent Schrödinger equation, and at each time step the whole instantaneous potential energy curve for the proton transfer is calculated. Details of the QCMD/AVB algorithm and its application for PLA_2 are described in [31]. Figure 15 presents fluctuations of the AVB energy profile for the proton transfer observed in the simulation. A short time interval, at which the transfer is initialized, was selected. QCMD trajectories starting from the enzyme–substrate complex thermalized and equilibrated in its initial state in the room temperature lead to the proton transfer after 2–8 ps. Typical quantum-classical (QCMD/AVB) and classical (MD/AVB) trajectories starting from the same initial states are compared in Figures 16 and 17. The first figure shows that the proton transfer occurs exclusively in the quantum dynamical model. This demonstrates the importance of the quantum-

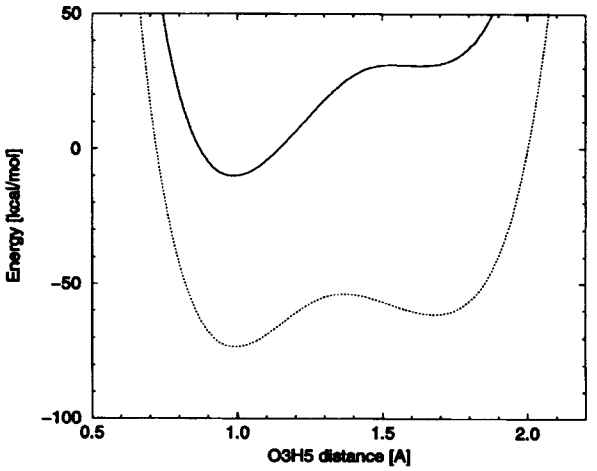

FIGURE 13. AVB energy profiles for the proton transfer in the model of the enzyme active site *in vacuo* (solid line) and in the presence of the point charge (+2) which mimics the presence of the Ca^{2+} ion (dotted line).

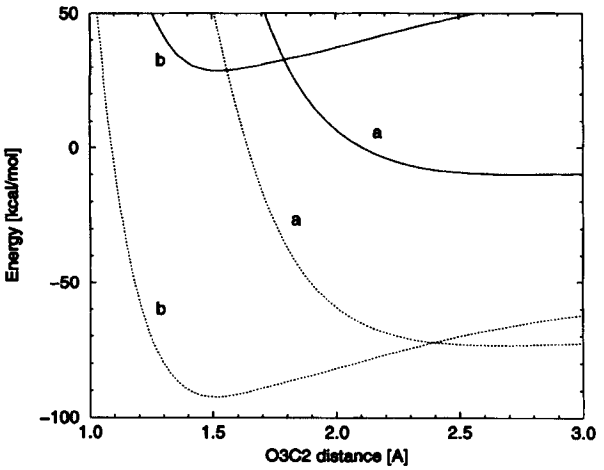

FIGURE 14. The AVB energy profiles for the attack of the water molecule on ester in (a) the planar configuration, and for the attack of hydroxyanion on ester in (b) the tetrahedral configuration. Solid and dotted lines refer to the calculations *in vacuo*, and in the presence of the point charge (+2) near the ester carbonyl group, respectively.

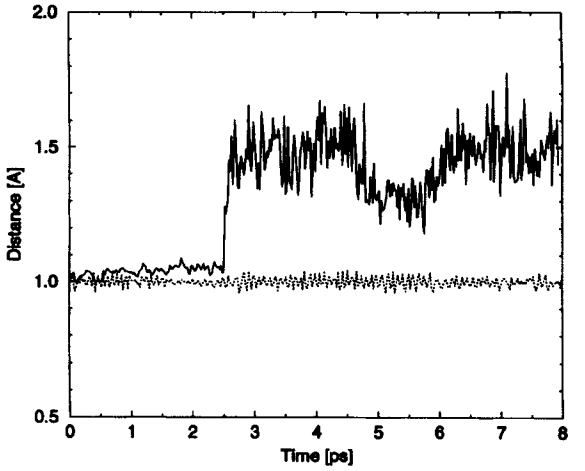

FIGURE 16. Changes of the distance between the O3 atom and the center of the H5 proton probability distribution in one of the QCMD / AVB simulations (solid line) and the changes of the corresponding classical MD / AVB trajectory (dotted line). The initial conditions for both simulations are the same, except the classical proton, which in the QCMD is replaced by the wave function.

dynamical effects for the enzymatic reaction under the study. The fluctuations of the C2O3 distance in the QCMD/AVB simulation which appear after the proton transfer are interpreted as attempts of the nucleophilic attack. These simulations have been carried out, and the results for longer time intervals are the subject of our next study [39].

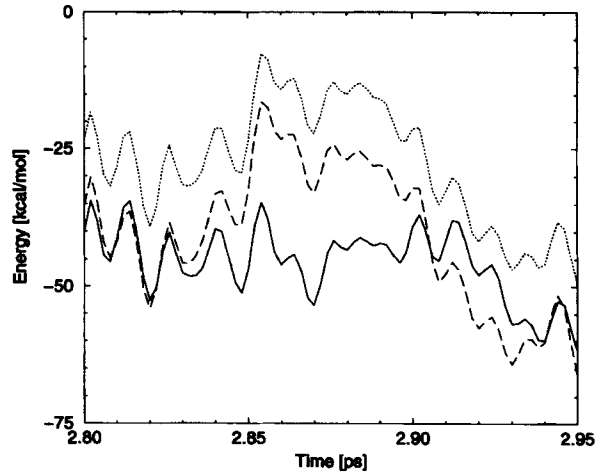

FIGURE 15. Selected points on the time-dependent AVB energy profile for the proton transfer. The solid, dotted, and dashed lines present the energy values in the first minimum of the profile (close to O3), in the maximum on the top of the barrier, and in the second minimum (close to N1), respectively. The proton transfer occurs approximately in the last 0.05 ps.

Conclusions

The microscopic AVB method was parametrized based on the DFT and conventional ab initio calculations. Some parameters were adjusted with respect to available experimental data in the gas phase for the water and imidazole molecules. The method was applied to study the enzymatic reaction catalyzed by PLA_2. Protein environment and solvent effects are included in the model via electrostatic interactions perturbing the original AVB Hamiltonian. The method was used as a fast potential energy function generator for the quantum-classical molecular dynamics (QCMD/AVB). The QCMD/AVB model allows, among others, for simulations of quantum-dynamical proton transfer and nucleophilic reactions in enzyme active sites and in solution. This study proposes a strategy for the parametrization procedure. The parameters can be refined using more advanced quantum-mechanical calculations as well as extended to other molecular and biomolecular systems, which is the subject of our further studies.

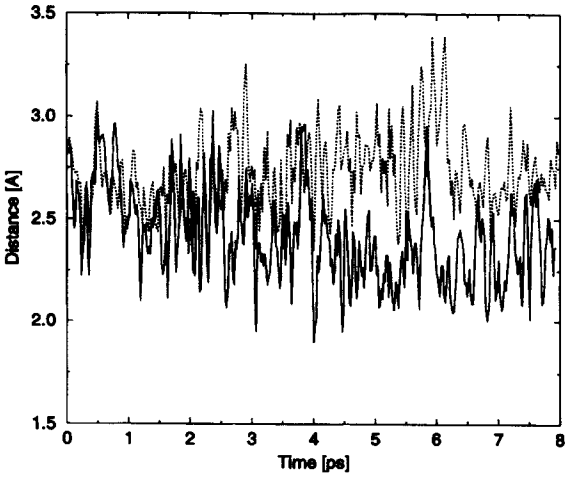

FIGURE 17. Distance between the O3 and C2 atoms demonstrating the progress of the nucleophilic attack. The QCMD / AVB (solid line) and MD / AVB (dotted line) trajectories were starting from the same initial conditions.

Appendix 1 Perturbation Expansion of the AVB Ground-State Energy

Consider a system described by a set of orthogonal valence states ψ_i. The Hamiltonian matrix $H_{ij} = \langle \psi_i | \hat{H} | \psi_j \rangle$ is assumed to be real-numbered and symmetric. Suppose its diagonal elements depend on a perturbation parameter λ. The total energy in the perturbed ground state, $\Psi = \Sigma_i c_i \psi_i$, can be expressed as follows:

$$E = \langle \Psi | \hat{H} | \Psi \rangle = \sum_{ij} c_i H_{ij} c_j, \tag{31}$$

c_i are real coefficients of the normalized eigenvector corresponding to the lowest eigenvalue of the Hamiltonian matrix:

$$\sum_j (H_{ij} - \delta_{ij} E) c_j = 0. \tag{32}$$

Derivative of (31) with respect to the perturbation parameter can be calculated as follows:

$$\frac{\partial E}{\partial \lambda} = \sum_{ij} c_i \frac{\partial H_{ij}}{\partial \lambda} c_j + 2 \sum_{ij} \frac{\partial c_i}{\partial \lambda} H_{ij} c_j = \sum_i \frac{\partial H_{ii}}{\partial \lambda} c_i^2. \tag{33}$$

In the first transformation we used the symmetry of the Hamiltonian matrix. In the second transformation we applied the assumption that the nondiagonal elements of the Hamiltonian matrix do not depend on the perturbation, and the following term vanishes based on (32) and the normalization condition:

$$2 \sum_{ij} \frac{\partial c_i}{\partial \lambda} H_{ij} c_j = 2 \sum_{ij} \frac{\partial c_i}{\partial \lambda} E c_i = E \frac{\partial}{\partial \lambda} \sum_{ij} c_i^2 = 0.$$

The analytical expression for the second-order derivative of the energy with respect to the perturbation parameter can be easily obtained for the two-state model. In the two-state model the squares of the coefficients c_i can be expressed with the aid of the ground-state energy and the diagonal elements of the Hamiltonian matrix, using (32) and the normalization condition (the prime symbols used previously in the text for the two-state diagonal elements are omitted):

$$c_1^2 = \frac{E - H_{22}}{2E - H_{11} - H_{22}}, \qquad c_2^2 = \frac{E - H_{11}}{2E - H_{11} - H_{22}}. \tag{34}$$

Equation (33) takes the form:

$$\frac{\partial E}{\partial \lambda}(2E - H_{11} - H_{22}) = \frac{\partial H_{11}}{\partial \lambda}(E - H_{22}) + \frac{\partial H_{22}}{\partial \lambda}(E - H_{11}).$$

One can take the derivative of both sides of the above equation with respect to λ and apply again Eqs. (33) and (34). One gets the following expression:

$$\frac{\partial^2 E}{\partial \lambda^2} = \frac{\partial^2 H_{11}}{\partial \lambda^2} c_1^2 + \frac{\partial^2 H_{22}}{\partial \lambda^2} c_2^2 + \frac{2 c_1^2 c_2^2}{H_{11} + H_{22} - 2E} \left(\frac{\partial H_{11}}{\partial \lambda} - \frac{\partial H_{22}}{\partial \lambda} \right)^2. \tag{35}$$

Consider now a particular case with the perturbation being the external electrostatic field **K**. Interaction of a neutral system with the external field can be approximated using the multipole expansion. In the simplest approach,

$$H_{ii} = H_{ii}^0 - k \mathbf{d}_i \mathbf{K}.$$

The effective dipole of the ground state can be calculated from (33):

$$\mathbf{d} := -\frac{1}{k}\left(\frac{\partial E}{\partial \mathbf{K}}\right)_{\mathbf{K}=0} = \sum_i \mathbf{d}_i c_i^2, \qquad (36)$$

where c_i are the coefficients of the normalized eigenvector of the unperturbed Hamiltonian matrix. Finally the effective polarizability of the two-state system in its ground state can be calculated from (35):

$$\hat{\alpha} := -\frac{1}{k}\left(\frac{\partial^2 E}{\partial \mathbf{K}^2}\right)_{\mathbf{K}=0} = \frac{2kc_1^2c_1^2\,\Delta\mathbf{d}\,\Delta\mathbf{d}^T}{H_{11}^0 + H_{22}^0 - 2E^0}, \qquad (37)$$

where $\Delta\mathbf{d} := \mathbf{d}_1 - \mathbf{d}_2$, and all other quantities correspond to the unperturbed Hamiltonian matrix.

ACKNOWLEDGMENT

This work was supported in part by the Polish State Committee for Scientific Research, the National Science Foundation, the Meta Center Program of NSF Supercomputer Centers, and the Curie-Sklodowska Foundation. The calculations were partially performed in the Interdisciplinary Centre for Mathematical and Computational Modelling at Warsaw University.

References

1. J. A. McCammon and S. C. Harvey, *Dynamics of Proteins and Nucleic Acids* (Cambridge University Press, Cambridge, 1987).
2. C. L. Brooks, M. Karplus, and B. M. Pettitt, in *Advances in Chemical Physics*, Vol. LXXI (Wiley, New York, 1988), pp. 1–259.
3. B. Lesyng and J. A. McCammon, Pharmac. Ther. **60**, 149 (1993).
4. P. Bala, B. Lesyng, and J. McCammon, Chem. Phys. **180**, 271 (1994).
5. P. Bala, B. Lesyng, and J. McCammon, Chem. Phys. Lett. **219**, 259 (1994).
6. P. Bala, P. Grochowski, B. Lesyng, and J. McCammon, Comp. Chem. **19**, 155 (1995).
7. W. Heitler and F. London, Z. Physik **44**, 455 (1927).
8. L. Pauling, *Nature of the Chemical Bond* (Cornell University Press, Ithaca, New York, 1960).
9. R. McWeeny, *Coulson's Valence* (Oxford University Press, Oxford, 1979).
10. J. N. Murrell, S. F. A. Kettle, and J. M. Tedder, *The Chemical Bond* (Wiley, Chichester, 1979).
11. A. Warshel and M. Weiss, J. Am. Chem. Soc. **102**, 6218 (1980).
12. A. Warshel and A. Lappicirella, J. Am. Chem. Soc. **103**, 4664 (1981).
13. A. Warshel, J. Phys. Chem. **86**, 2218 (1982).
14. A. Warshel and S. Russel, J. Am. Chem. Soc. **108**, 6569 (1986).
15. J. K. Hwang, G. King, S. Creighton, and A. Warshel, J. Am. Chem. Soc. **110**, 5297 (1988).
16. A. Warshel and Z. T. Chu, J. Chem. Phys. **93**, 4003 (1990).
17. A. Warshel, *Computer Modelling of Chemical Reactions in Enzymes and Solutions* (Wiley, New York, 1991).
18. J. Aqvist and A. Warshel, Chem. Rev. **93**, 2523 (1993).
19. F. Bernardi, M. Olivucci, and M. A. Robb, J. Am. Chem. Soc. **114**, 1606 (1992).
20. M. J. Bearpark, M. A. Robb, F. Bernardi, and M. Olivucci, Chem. Phys. Lett. **217**, 513 (1994).
21. M. J. Field, P. A. Bash, and M. Karplus, Comp. Chem. **11**, 700 (1990).
22. D. Arad, R. Langridge, and P. A. Kollman, J. Am. Chem. Soc. **112**, 2860 (1990).
23. H. J. C. Berendsen and J. Mavri, J. Phys. Chem. **97**, 13464 (1993).
24. R. Alimi, R. B. Gerber, A. D. Hemmerich, R. Kosloff, and M. A. Ratner, J. Chem. Phys. **93**, 6484 (1990).
25. D. C. Borgis, S. Lee, and J. T. Hynes, Chem. Phys. Lett. **162**, 19 (1989).
26. D. Borgis and J. T. Hynes, Chem. Phys. **170**, 315 (1993).
27. N. Makri and W. H. Miller, J. Chem. Phys. **91**, 4026 (1989).
28. W. H. Miller, in *Molecular Aspects of Biotechnology: Computational Models and Theories* (Kluwer Academic Publishers, Dordrecht, 1992), pp. 149–167.
29. J. N. Onuchic, R. F. Goldstein, and W. Bialek, in *Perspectives in Photosynthesis* (Kluwer Academic Publishers, Dordrecht, 1990), p. 211.
30. R. Car and M. Parinello, Phys. Rev. Lett. **55**, 2471 (1985).
31. P. Bala, P. Grochowski, B. Lesyng, and J. McCammon, in *Quantum Mechanical Simulation Methods for Studying Biological Systems*, Les Houches Physics School series, (Springer-Verlag, Berlin, 1996), pp. 119–156.
32. S. P. White, D. L. Scott, Z. Otwinowski, M. H. Gelb, and P. B. Sigler, Science **250**, 1560 (1990).
33. D. L. Scott, S. P. White, Z. Otwinowski, W. Yuan, M. H. Gelb, and P. B. Sigler, Science **250**, 1541 (1990).
34. L. Hedin and B. I. Lundqvist, J. Phys. **4**, 2064 (1971).
35. M. Kieninger and S. Suhai, Int. J. Quant. Chem. **52**, 465 (1994).
36. V. Barone, L. Orlandini, and C. Adamo, Chem. Phys. Lett. **231**, 295 (1994).
37. U. Ch. Singh and P. A. Kollman, J. Comp. Chem. **5**, 129 (1984).
38. L. E. Chirlian and M. Miller Francl, J. Comp. Chem. **8**, 894 (1987).
39. P. Bala, P. Grochowski, B. Lesyng, and J. A. McCammon, J. Phys. Chem., in preparation.
40. G. Bakalarski, P. Grochowski, J. S. Kwiatkowski, B. Lesyng, and J. Leszczynski, Chem. Phys. (1996), to appear.